JOURNAL OF THE MECHANICAL BEHAVIOR OF BIOMEDICAL MATERIALS 65 (2017) 356–372

Available online at www.sciencedirect.com

ScienceDirect

www.elsevier.com/locate/jmbbm

Research Paper

Endothelial pattern formation in hybrid constructs of additive manufactured porous rigid scaffolds and cell-laden hydrogels for orthopedic applications

Yaser Shanjani[a], *Yunqing Kang*[a,1], *Livia Zarnescu*[b], *Audrey K. (Ellerbee) Bowden*[c], *Jeong-Tae Koh*[d], *Dai Fei Elmer Ker*[a], *Yunzhi Yang*[a,b,e,*]

[a]*Department of Orthopedic Surgery, Stanford University, 300 Pasteur Drive, Stanford, CA 94305, USA*
[b]*Department of Bioengineering, Stanford University, 318 Campus Drive, Stanford, CA 94305, USA*
[c]*Department of Electrical Engineering, Stanford University, 348 Via Pueblo, Stanford, CA 94305, USA*
[d]*School of Dentistry, Chonnam National University, 77 Yongbong-ro, Buk-gu, Gwangju 500-757, Republic of Korea*
[e]*Department of Materials Science and Engineering, Stanford University, 300 Pasteur Drive, Stanford, CA 94305, USA*

ARTICLE INFO

Article history:
Received 8 April 2016
Received in revised form
26 August 2016
Accepted 27 August 2016
Available online 4 September 2016

Keywords:
Additive manufacturing
Scaffold
Hydrogel
Endothelial cell
Cell network pattern

ABSTRACT

Vascularization of tissue engineering constructs (TECs) *in vitro* is of critical importance for ensuring effective and satisfactory clinical outcomes upon implantation of TECs. Biomechanical properties of TECs have remarkable influence on the *in vitro* vascularization of TECs. This work utilized *in vitro* experiments and finite element analysis to investigate endothelial patterns in hybrid constructs of soft collagen gels and rigid macroporous poly(ε-caprolactone)-β-tricalcium phosphate (PCL-β-TCP) scaffold seeded/embedded with human umbilical vein endothelial cells (HUVECs) for bone tissue engineering applications. We first fabricated and characterized well-defined porous PCL-β-TCP scaffolds with identical pore size (500 μm) but different strut sizes (200 and 400 μm) using additive manufacturing (AM) technology, and then assessed the HUVEC's proliferation and morphogenesis within collagen, PCL-β-TCP scaffold, and the collagen-scaffold hybrid construct. Results showed that, in the hybrid construct, the cell population in the collagen component dropped by day 7 but then increased by day 14. Also, cells migrated onto the struts of the scaffold component, proliferated over time, and formed networks on the thinner struts (i.e., 200 μm). Also, the thinner struts resulted in formation of long linear cellular cords structures within the pores. Finite element simulation demonstrated principal stress patterns similar to the observed cell-network pattern. It is probable that the scaffold component modulated patterns of principal stresses in the collagen component as

*Correspondence to: Department of Orthopedic Surgery, School of Medicine, Stanford University, 300 Pasteur Drive Edwards R155, Stanford, CA 94305, USA. Fax: +650 724 5401.
E-mail address: ypyang@stanford.edu (Y. Yang).
[1]Current address: Department of Ocean and Mechanical Engineering, Florida Atlantic University, Boca Raton, FL 33431, USA.

http://dx.doi.org/10.1016/j.jmbbm.2016.08.037

biomechanical cues for reorganization of cell network patterns. Also, the scaffold component significantly improved the mechanical integrity of hydrogel component in the hybrid construct for weight-bearing applications. These results have collectively indicated that the manipulation of micro-architecture of scaffold could be an effective means to further regulate and guide desired cellular response in hybrid constructs.

1. Introduction

Lack of proper vascularization of tissue engineering constructs (TECs) causes cellular necrosis in the inner regions and failure of the engineered tissues after implantation (Lovett et al., 2009; Sakaguchi et al., 2013; Auger et al., 2013; Mercado-Pagan et al., 2015). *In vitro* prevascularization of TECs prior to implantation holds great promise to improve cell viability and overcome center necrosis of large TECs via facilitating the rapid establishment of microcirculation, and enhancing tissue engraftment, integration and regeneration *in vivo* (Levenberg et al., 2005; Chen et al., 2009; Fedorovich et al., 2010). Hydrogels made of extracellular matrix-like polymers provide a suitable environment for formation of capillary network *in vitro* (Hanjaya-Putra et al., 2011; Lloyd-Griffith et al., 2015; McFadden et al., 2013; Duffy et al., 2011; Correia et al., 2011; Leong et al., 2013). For instance, McFadden et al. McFadden et al., (2013) demonstrated *in vitro* prevascularization of a collagen-GAG matrix using human umbilical vein endothelial cells (HUVECs) and Mesenchymal stem cells (MSCs). Also, Duffy et al. (2011) achieved capillary-like networks *in vitro* by using MSCs cultured with endothelial supplements within collagen-glycosaminoglycan scaffolds. However, in general, the mechanical properties of such hydrogels are far below those of load-bearing bone tissues (Tian and George, 2011), and their pre-formed TECs are less convenient for surgical manipulation (Gong et al., 2007). Therefore, for load-bearing bone TECs, it is highly desirable and beneficial to combine a rigid porous scaffold of appropriate mechanical properties and a soft cell-laden hydrogel matrix to promote *in vitro* prevascularization within a mechanically-sound structure. In such hybrid constructs, in addition to support mechanically, the scaffold component provides micro-architectural guidance for cells to reorganize and form vascular networks in hydrogel within porous scaffold. A few studies have reported the *in vitro* cellular network formation in such hybrid constructs (Gong et al., 2007; Melchels et al., 2012; Schuurman et al., 2011; Kim et al., 2012; Mintz and Cooper, 2014; de Moraes et al., 2012; Santos et al., 2008), however, the biomechanical effects of both soft and rigid components of hybrid construct on the cellular behavior and reorganization of cells for network formation are poorly understood.

The objective of this study is to investigate the *in vitro* endothelial cell pattern and network formation as well as the reciprocal biological and biomechanical effects between endothelial cells and environment provided within a hybrid bone tissue engineering construct. To control the microstructures of the construct such as porosity, pore size and strut size of the scaffold component, we utilized additive manufacturing (AM) technology for fabrication of rigid porous scaffolds. AM technology enabled us to fabricate porous scaffolds with well-defined geometry and highly-reproducible controlled porous architecture in contrast with conventional scaffolding fabrication methods (Melchels et al., 2012; Yang et al., 2002; Mota et al., 2015). We used a biodegradable composite of poly(ε-caprolactone) (PCL) and β-tricalcium phosphate (β-TCP) for the rigid scaffold component and collagen as the soft hydrogel matrix because PCL-β-TCP has been extensively used for bone tissue engineering (Lim et al., 2011; Yeo et al., 2010; Macedo et al., 2012; Sawyer et al., 2009; Yeo et al., 2008), and collagen hydrogel has been widely used as an extracellular matrix carrier for *in vitro* vasculature formation (Kang et al., 2015; Cen et al., 2008; Garvin et al., 2011; Deng et al., 2010). We characterized the structural and mechanical properties of the scaffold and hydrogel components. Then, we loaded HUVECs into a collagen precursor solution and casted the cell-containing solution on the porous scaffolds for subsequent gelation. Finally, we studied the formation of endothelial networks across the hybrid constructs and the effect of scaffolds with different strut size on network morphogenesis.

2. Materials and methods

2.1. Materials

Medical-grade PCL (mPCL) pellets (Sigma Aldrich, St Louis, MO) with density of 1.145 g/cm^3 (Mn=80,000) were used as received. β-TCP powder with a specific surface area of 17 m^2/g and particle size of mesh 60 was obtained from Nanocerox, Inc. (Ann Arbor, Michigan). A slurry was prepared by dispersing β-TCP powder in acetone at 50 °C, followed by gradual incorporation of PCL pellets. A PCL:β-TCP:acetone weight ratio of 80:20:400 was used. Vigorous mechanical stirring was performed for 3 h to ensure the homogenous distribution of the β-TCP particles in the PCL slurry. The slurry was poured out evenly into glass plates, left overnight to evaporate, and further dried in a vacuum overnight to remove any residual acetone. Then, the material was warmed up and extruded through a 2.2 mm orifice to form filaments for AM of scaffolds. Collagen type I solution (Cellmatrix Type I-A; 3 mg/mL in DPBS; pH = 7.4, Nitta Gelatin) was purchased from Wako Chemicals USA, Inc. (Richmond, VA) for hydrogel component of hybrid constructs.

Table 1 – Structural characteristics of scaffolds ($n=20$).

Strut size		200 μm	400 μm
Strut Size (μm)	Design	200	400
	SEM measurement	260.3±21.5	442.1±16.2
	Deviation[a]	30.2%	10.5%
Pore Size (μm) – in layers plane	Design	500	500
	SEM measurement	441.1±20.6	444.8±24.3
	Deviation[a]	−11.8%	−11.0%
Pore Size (μm) – in perpendicular plane	Design	130	300
	SEM measurement	108.5±11.4	249.0±26.8
	Deviation[a]	−16.6%	−17.0%

[a] Deviation=(Measured value − Design)/Design × 100.

2.2. Fabrication of PCL-β-TCP scaffold

The filaments were fed into our in-house-built Hybprinter (Shanjani et al., 2015) where they were melted at 140 °C, extruded as tiny struts and laid down in 0/90° patterns layer-upon-layer to form porous lattice-shaped scaffolds. To investigate the effect of scaffold geometrical features on cells' behavior and network development, scaffolds with constant pore size and different strut size were designed. Two types of PCL-β-TCP scaffolds were formed and characterized: scaffolds with 200 and 400 μm strut size with, respectively, 165, and 350 μm layer thickness (=distance between the sequential layers). The porosity of the scaffolds was adjusted via the operating software in a way to make pore size (=spacing between the edge of struts in the plane of each layer) equal to 500 μm. For that purpose, the porosity of the structures with 200 and 400 μm strut size was designated as 67%, and 57%, respectively (Table 1). All scaffolds were surface-treated in 5 M NaOH for 18 h at room temperature to enhance their hydrophilicity to improve penetration of the cell-laden collagen into the pores and mechanical interlock between collagen and strut surfaces during integration of pliant collagen gels with rigid PCL-β-TCP scaffolds.

2.3. Structural characterization of PCL-β-TCP scaffolds

Porous PCL-β-TCP scaffolds were scanned by a high-resolution micro-computed tomography (micro-CT) machine (Skyscan1172, Scanco Medical, Basserdorf, Switzerland). The CT scanner was set to operate at 49 kV voltage, 200 μA current and 17 μm resolution. Porosity and specific surface area of the scaffolds were calculated with NRecon 1.4.4 software. The scan images were also used for 3D reconstruction and visual observation of the microstructures. AM-made scaffolds were also scanned via secondary electron emission imaging using SEM (FEI XL30 Sirion) to analyze strut size, pore size, and layer thickness as well as to observe surface morphology of the struts. Three samples per group were used. The PCL-β-TCP scaffolds were first sputter-coated with gold (10 nm; SPI Sputter, SPI Supplier Division of Structure Prob Inc., West Chester, PA, USA) to make them electrically conductive. The SEM acceleration voltage was set to 5 kV.

2.4. Water-uptake measurement

To investigate the effect of surface treatment on the hydrophilicity of PCL-β-TCP scaffolds, their water-uptake capability was tested. The water-uptake characteristic may also represent the surface condition of the scaffold struts for collagen mechanical integration as well as cell adhesion and proliferation (Yeo et al., 2012). The water uptake ability of the porous scaffolds was determined by completely immersing the samples in distilled water for 60 s. The bulk water accumulated on the outer surfaces of the samples was removed via blotting with a piece of wet filter paper. Then, the wet scaffolds were weighed immediately using an electronic balance (XS105, METTLER TOLEDO, Columbus, OH). The percentage of water uptake was determined as

$$\text{Water Uptake } \% = \frac{W_w - W_d}{W_d} \times 100$$

where W_w and W_d are the weight of wet and dry samples, respectively. The test was conducted using five specimens of each sample type (i.e., different strut size). Each measurement was triplicated for each scaffold and the average value was calculated.

2.5. Mechanical testing

The mechanical properties of the scaffolds were measured using an Instron 5944 uniaxial testing system with a 2 kN load-cell (Instron Corporation, Norwood, MA). Specimens with 5×5 mm^2 square cross-section and 10 mm in height were mechanically tested under compression between two platens (one self-aligning, one fixed) at a speed of 0.1% strain/sec up to 25% strain with 1 N preload. Displacement was determined from an extensometer (Epsilon Technology Corp, Jackson WY) attached to the two platens. Five samples were tested for each group of 200 and 400 μm strut size. The testing protocol was adapted from the reference (Zein et al., 2002) where, for all the specimens, the apparent modulus of elasticity was calculated as the slope of the initial linear portion of the stress-strain curve. The effective stress values were determined as the compressive loading value per the apparent initial cross-sectional area of each test specimen. The strain values were calculated via dividing the deformation values with the initial specimen height. Yield compression strength was defined as the intersection of the stress-strain curve with a line with a slope equal to the modulus starting at an offset of 1% strain.

We also measured the compressive modulus of the collagen gel matrix through unconfined compression tests using an Instron 5944 materials testing system (Instron Corporation, Norwood, MA) fitted with a 1 N load cell (Interface Inc., Scottsdale, Az). The test set-up consisted of custom-made aluminum compression platens lined with PTFE to minimize friction. All tests were conducted in phosphate buffered saline (PBS) solution at room temperature. Gel discs of 8 mm in diameter and 3 mm in thickness were tested. The specimen dimensions were measured using digital calipers (diameter) and by readout of the testing system's position (height). Before each test, a preload of approximately 1 mN was applied. The upper platen was then lowered at a rate of

0.1% strain/sec to a maximum strain of 30%. Load and displacement data were recorded at 100 Hz. The compressive modulus was determined for strain ranges of 10-20% from linear curve fits of the stress vs. strain curve in each strain range.

2.6. Preparation of HUVECs

Human umbilical vein endothelial cells (HUVECs) expressing green fluorescent protein (GFP) were generously gifted by the late Dr. J. Folkman (Children's Hospital, Boston) and used for cell culture in this study. HUVECs were cultured in endothelial basal medium (EBM-2, Lonza Inc., Hopkinton, MA) with endothelial growth supplement SingleQuots (EGM-2, Lonza Inc., Hopkinton, MA) in a 5% CO_2 atmosphere at 37 °C. Upon about 85-90% confluence, HUVECs were subcultured using 0.25% trypsin-EDTA (Invitrogen, USA) and resuspended in EBM culture medium.

2.7. Fabrication of hybrid constructs

Surface-treated scaffolds ($6 \times 6 \times 2$ mm^3 with 200 and 400 μm strut size) were washed three times using PBS and sterilized by 70% ethanol solution. For prewetting, the PCL-β-TCP scaffolds were immersed in cell culture medium overnight. The prewetted scaffolds then were placed in a non-treated 48 well-plate. 1×10^6 cells were suspended in 200 μl of the collagen solution and loaded onto the individual scaffolds in each well. The amount of collagen solution was sufficient to fill the pores of the scaffold and cover its top surface. After 30 min incubation, the cell-laden collagen hydrogel gelled and encapsulated HUVECs in the collagen-scaffold hybrid construct. Fresh EBM medium was then added for further incubation. The same amount of cell-laden collagen was casted in empty culture wells (without scaffold) to form control collagen matrix. In addition, 1×10^6 cells in 1 ml culture medium were seeded directly into the PCL-β-TCP scaffolds (without collagen) and incubated at 37 °C as control scaffold samples. Every 15 minutes (for 1 h), the scaffolds were flipped over to allow cells to homogenously attach onto the struts of the scaffolds. Morphology of GFP-tagged cells was monitored in hybrid constructs, control collagen and on control scaffolds 6 h after seeding using a Zeiss fluorescent microscope (Jena, Germany). Three samples from each scaffold type (i.e., 200 μm and 400 μm strut size) were used for cell culture and further biological studies. Culture medium was changed every two days for all the samples.

2.8. Cell migration and proliferation assay

We quantified the number of cells encapsulated within the collagen component and attached on the scaffold component of the hybrid construct at 1, 7 and 14 days of culture to investigate the rate of migration from the soft collagen matrix onto the rigid struts and proliferation on them as well as the rate of proliferation of remaining HUVECs in the collagen. The initial cell density was 5×10^6/ml and the total number of seeding cells for each sample was 1×10^6. To this end, the cell-laden collagen component of the hybrid construct was digested with a 2 mg mL^{-1} collagenase-A solution (Roche Applied Science, Indianapolis, IN, USA) for 4 h at 37 °C. Then, the cells on the scaffold component were trypsinized (200 μl for each sample) for half an hour and collected after adding 300 μl of EBM. The retrieved cells were counted using a Z2 Coulter counter (Beckman Coulter, Miami, Fl). The test was also performed on the control scaffold samples and control collagen with identical initial number of seeding cells, and the results were compared with the hybrid constructs. For this test, based on our extensive cellular evaluation experience, 48 well plates were chosen to contain all 5 types of samples (including 200- and 400 -μm collagen-scaffold constructs, control 200- and 400-μm scaffolds and control collagen) per condition/batch to reduce potential discrepancy among sample preparation and cellular conditions. The structure of the scaffolds was the same as used in mechanical test i.e., scaffolds were composed of same 200- and 400 -μm struts with same spacing and layer thickness, though we selected smaller overall dimensions of scaffolds to fit in the 48 well plate. We conducted two repeat studies on cell viability and proliferation with 3 samples each time; thus, the overall n equals 6 (3 sample/time × twice).

2.9. F-actin staining for cell morphology

Rhodamine phalloidin was used to stain cells' F-actin to assess cytoskeletal organization on the collagen/PCL-β-TCP hybrid constructs, control PCL-β-TCP scaffolds, and control collagen hydrogel. After 2 and 7 days of incubation, the cells/constructs were rinsed twice using PBS, and then fixed by 4% paraformaldehyde solution (PFA) for 15 min at room temperature. The fixed cells were further permeabilized in 0.5% Triton X-100, and incubated in 100 nM rhodamine phalloidin working solution (Cytoskeleton Inc. USA) for 2 h at room temperature. After a quick rinse with PBS, DAPI solution (5 μg/mL) was added to counterstain cell nuclei. After thorough washing with PBS, cells were observed under a Zeiss fluorescent microscope.

2.10. Immunofluorescent staining of PECAM-1 (CD31)

Immunofluorescent staining of platelet-endothelial cell adhesion molecule (PECAM-1, or CD31) was performed using an established procedure to investigate the inter-cellular connections and to observe network formation of HUVECs on the collagen/PCL-β-TCP hybrid constructs, control PCL-β-TCP scaffolds, and control collagen hydrogel. After 14 days of culture, the cell/constructs were fixed in a solution of 4% PFA for 15 min at room temperature. After washing three times in PBS, the samples were placed in 5% bovine serum albumin (BSA)/PBS blocking buffer for 1 h, and then were incubated with mouse anti-human CD31 primary antibody (1:3200, Cell Signaling Technology, Danvers, MA) in 1% BSA/PBS overnight at 4 °C. The cells/scaffolds were then washed three times using PBS, and incubated in an anti-mouse secondary antibody Alexa Fluor® 594 (1:1000; 2 μg/mL, Invitrogen, Carlsbad, CA) for 1 h at room temperature. After rinsing the samples

using PBS, the cell nuclei were counterstained with DAPI solution (5 μg/mL) for 1 min. The scaffold samples were then extensively washed with PBS, and visualized by a Zeiss fluorescent microscope.

2.11. *Optical coherence tomography (OCT)*

The internal structure of the hybrid collagen/PCL-β-TCP scaffolds were observed at day 14 using a commercially available

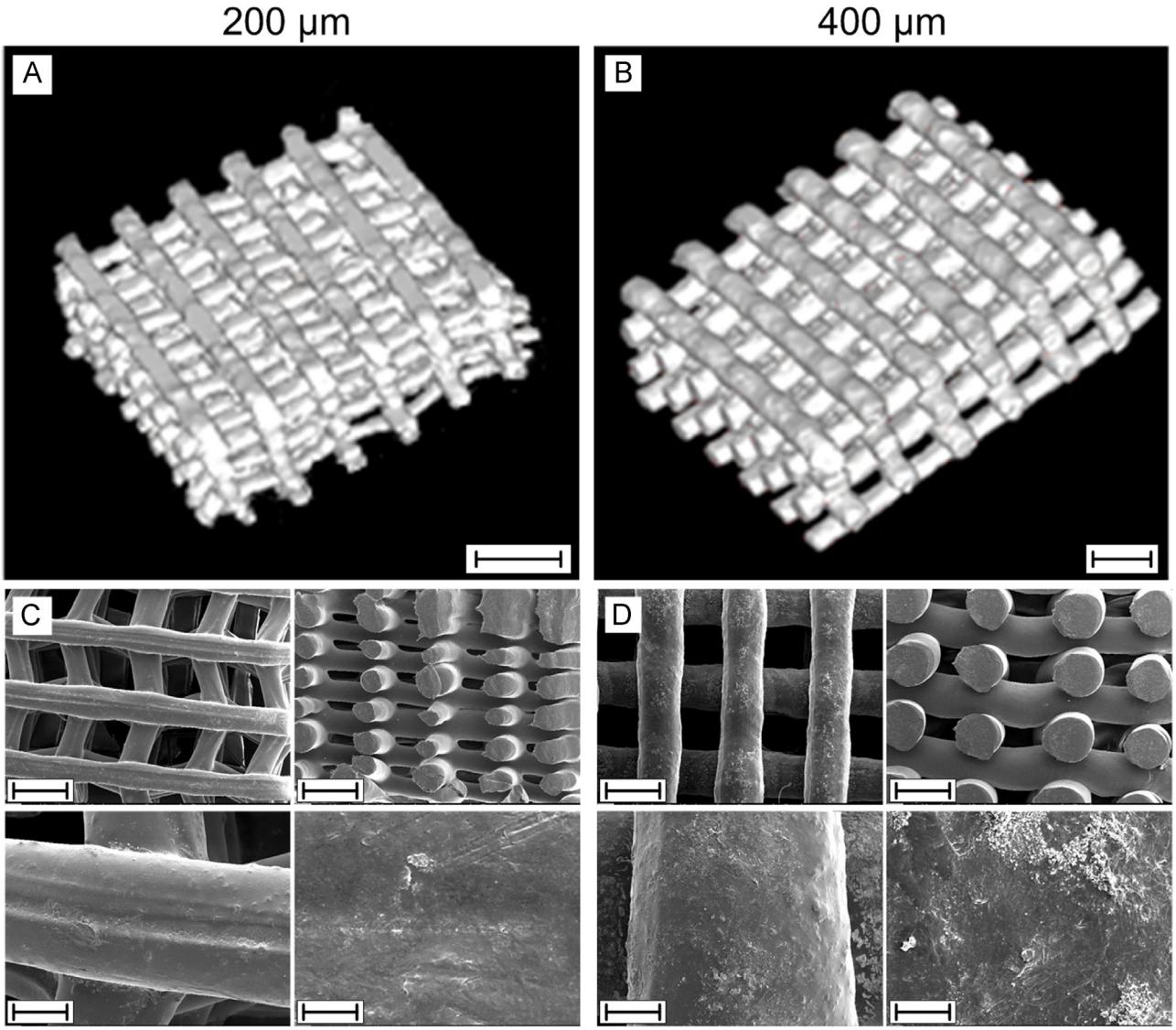

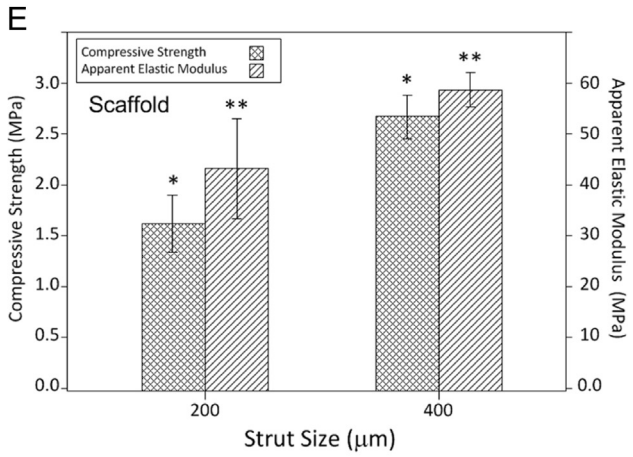

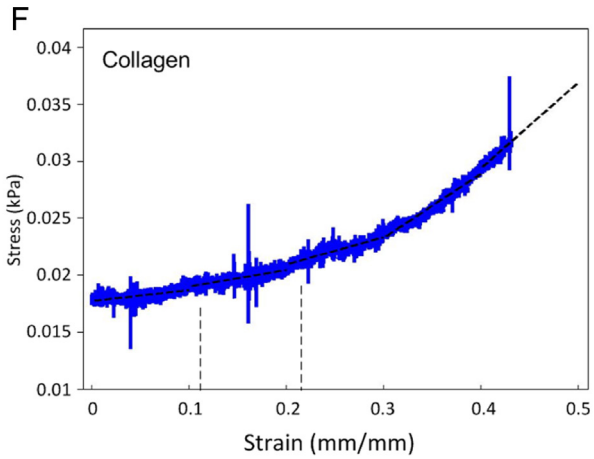

optical coherence tomography (OCT) system: Telesto OCT Imaging Systems (1310 nm, maximum 92 kHz line rate, 5.5 μm axial resolution, Thorlabs Inc., Newton, NJ). Also, the morphology of the cells and lumen formation in the collagen component close to the top surface were investigated after 14 days culture using a custom-built high resolution full-field OCT system (1.5 μm axial resolution, 1 μm lateral resolution, 580 nm) (Zarnescu et al., 2015). No staining was required for OCT imaging.

2.12. Dimension change of collagens in presence and absence of cells

We measured the geometrical variation of collagen matrix in the presence and absence of cells over time as an indicator to indirectly estimate the effect of cellular traction force on the collagen matrix. For this purpose, collagen hydrogel disks of 8 mm in diameter were formed with and without (as control) encapsulated ECs (initial cell density 5×10^6/ml) using cylindrical molds. The selection of 8 mm was because it is a close estimation of the diameter of individual wells of 48 well plate minus the curved edge of collagen gel concave meniscus occurs in the well. The disks were floated in EBM. The diameter of the disks was measured over time up to 14 days of culture. The dimensional change of collagen-only samples (without cells) was used as an estimation of material degradation, and the variation of such dimension in cell-laden collagen samples in comparison with the collagen-only (without cells) disks was used as an estimate of the bulk effect of cellular traction force.

2.13. Finite element analysis of cell mediated collagen contraction

A simplified finite element model (FEM) was developed on the basis of cell-mediated contraction and the mechanical constrains on the collagen matrix in the hybrid constructs to rationalize and validate the observed pattern of EC network. To model the cell-mediated contraction effect, a pre-described displacement boundary condition was applied to the top surface of the hydrogel component used as inputs for the FEM. The pre-described boundary displacement was defined based on the shape of hybrid construct obtained by OCT and the cell-mediated shrinkage percentage determined by previous dimension change test (as described in Section 2.12). The scaffold struts and the well plate wall and bottom were modeled as fixed mechanical constrains due to adhesion of collagen to those surfaces. The meniscus shape due to surface tension between initial collagen solution and well plate was simplified to a flat surface due to the lack of information about the exact profile of the meniscus. The stiffness of the collagen matrix, which was measured via mechanical testing, was used in this model. One quarter of the hybrid hydrogel-scaffold was modeled in the FEM software package COMSOL Multiphysics 4.3 and a linear elastic material model was utilized for simulation. The mesh accuracy of the model was tested via mesh refining method. The spatial distribution of principal stress in the hydrogel component was calculated.

2.14. Statistical analysis

The values reported for the mechanical test, water-uptake measurement and cell proliferation assay are presented as the mean values ± the standard deviation (STD). For mechanical and water-uptake tests, the difference was considered statistically significant as analyzed by a t-test if the p-value was less than 0.05. For the cell proliferation study, one-way analysis of variance (ANOVA) with post-hoc Tukey's test ($p < 0.05$) was used for the migration and proliferation test.

3. Results

3.1. Structural characteristics and morphology

Reconstructed 3D models of the 200- and 400 -μm strut scaffolds generated by micro-CT scanning are shown in Fig. 1(A) and (B), respectively. Also, the SEM images of horizontal and vertical cross sections (parallel and perpendicular to the layers) of the scaffolds with different strut size are shown in Fig. 1(C) and (D), demonstrating well-defined layers of struts and interconnected pores of the scaffolds. The strut size, pore size, and layer thickness were measured using the SEM images, and deviations from the original designs are listed in Table 1. The geometrical deviations from the original designs of the strut sizes and pore size (parallel and perpendicular to layers) were determined, showing that the struts were formed ~40–60 μm larger than the original design in AM-operating software (i.e., 10–30% deviation). Consequently, the pores in the layers plane were built about 55–60 μm smaller than 500 μm (i.e., approximately 11% deviation). Despite the dimensional deviations, the pore sizes remained consistent (i.e., measured ~450 μm) for all the structures with different strut sizes.

Table 2 lists the porosity and specific surface area of the scaffolds that were quantified by the micro-CT analysis. The porosity and specific surface area of the scaffolds were in reasonable agreement with the original CAD design despite

Fig. 1 – Structural and mechanical properties of constituent components of TEC: (A) and (B) reconstructed 3D model of 200- and 400 -μm scaffolds, respectively, generated using micro-CT scanning. Bars equal 1 mm. (C) and (D) low and high magnification SEM micrographs of horizontal and vertical cross sections (parallel and perpendicular to the layers) of the AM-made PCL-β-TCP scaffolds with 200- and 400 -μm struts, respectively. Bars equal 500 μm in the top row images while represent 100 μm and 10 μm in the bottom row in left and right columns, respectively. (E) mechanical strength and apparent modulus of elasticity of scaffolds measured under compression until 1% strain and ($n = 5$). Both mechanical properties are significantly different for 200- and 400-μm scaffolds as indicated by * and ** considering $p < 0.05$, (F) stress-strain curve of collagen matrix under compression. Modulus of elasticity was calculated equal to 12.08 ± 2.86 Pa for 10–20% strain range.

Table 2 – Physical characteristics of scaffolds.

Strut size		200 μm	400 μm
Porosity (%)	CAD	67	57
	μCT measurement	68.8	53.6
	Deviation[a]	2.6%	−5.9%
Surface area/volume (1/mm)	CAD[a]	20	9
	μCT measurement	18.2	10.8
	Deviation	−9.1%	19.5%
Water uptake (%) ($n=5$)	Before surface treatment	19.6±3.5	14.8±1.7
	After surface treatment	100.9*±12.6	64.3±2.8
	% of increase	414.3%	332.9%

[a] Deviation = (Measured value − CAD)/CAD × 100.
* 200 μm was significantly different from 400 μm struts with $p<0.05$.

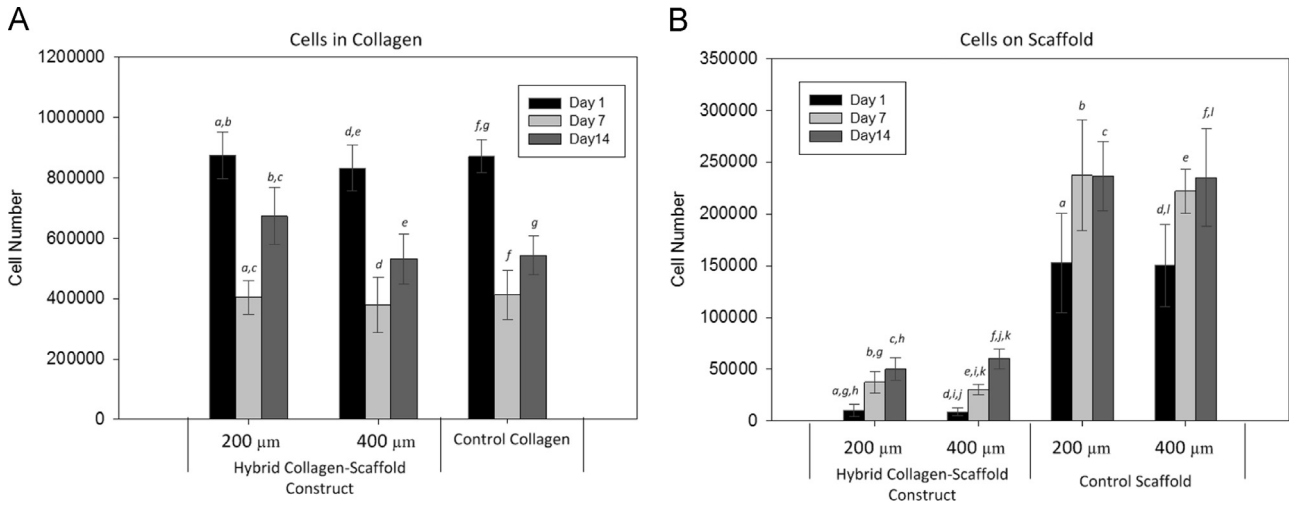

Fig. 2 – Proliferation rate of HUVECs (A) in collagen component and (B) on of PCL-β-TCP scaffold components of hybrid constructs: The left two sets of (A) represent the number of cells counted within the collagen component of hybrid construct with 200- and 400 -μm struts over time that are comparable with the number of the cells in the control collagen. The left two sets of (B) represent the number of cells on the struts of the scaffold component over time. Other two sets of data on the right of (B) represent the number of cells on the control scaffolds ($n=6$). Groups with the same small letters are significantly different from each other with $p<0.05$.

the abovementioned geometrical deviations in strut and pore size. The porosity and specific surface area of the samples formed with smaller struts (smaller diameter) were higher than those of bigger struts. Also, overnight alkaline treatment significantly increased water-uptake of the scaffolds (300–400%) regardless of strut size (Table 2).

3.2. *Mechanical properties*

The strength and apparent modulus of elasticity of PCL-β-TCP scaffolds with different strut size were measured under compression. As shown in Fig. 1(E), the strength of the scaffolds falls in the range of 1.6–2.6 MPa which is comparable with the strength of human trabecular bone (An, 2000). The apparent modulus of the scaffolds is in the range of 42–58 MPa. The scaffolds with the thinner strut size exhibited significantly lower compressive strength and apparent elastic modulus. This behavior is attributed to the higher porosity and smaller fusion joints between struts of the sequential layers. The compressive modulus of the collagen matrix was 12.08±2.86 Pa in 10–20% strain range (as depicted in Fig. 1(F)), which is comparable with the reported values in literature (Wu et al., 2005).

3.3. *Cells in hybrid constructs*

Proliferation of cells in the hybrid constructs, control collagens and control scaffolds were quantified and compared (Fig. 2(A) and (B)). In the hybrid constructs, cell numbers were counted and reported separately in the collagen component and on the struts of the PCL-β-TCP scaffold component. The same total number (1×10^6) of initial seeding cells was applied to each sample regardless of hybrid constructs, control collagens and control scaffolds. As demonstrated in Fig. 2(A), at day 1 about 86–93% of cells were retrieved from digested control collagen matrix and collagen component of hybrid constructs. However, this number decreased to approximately 52% by day 7. Then, about

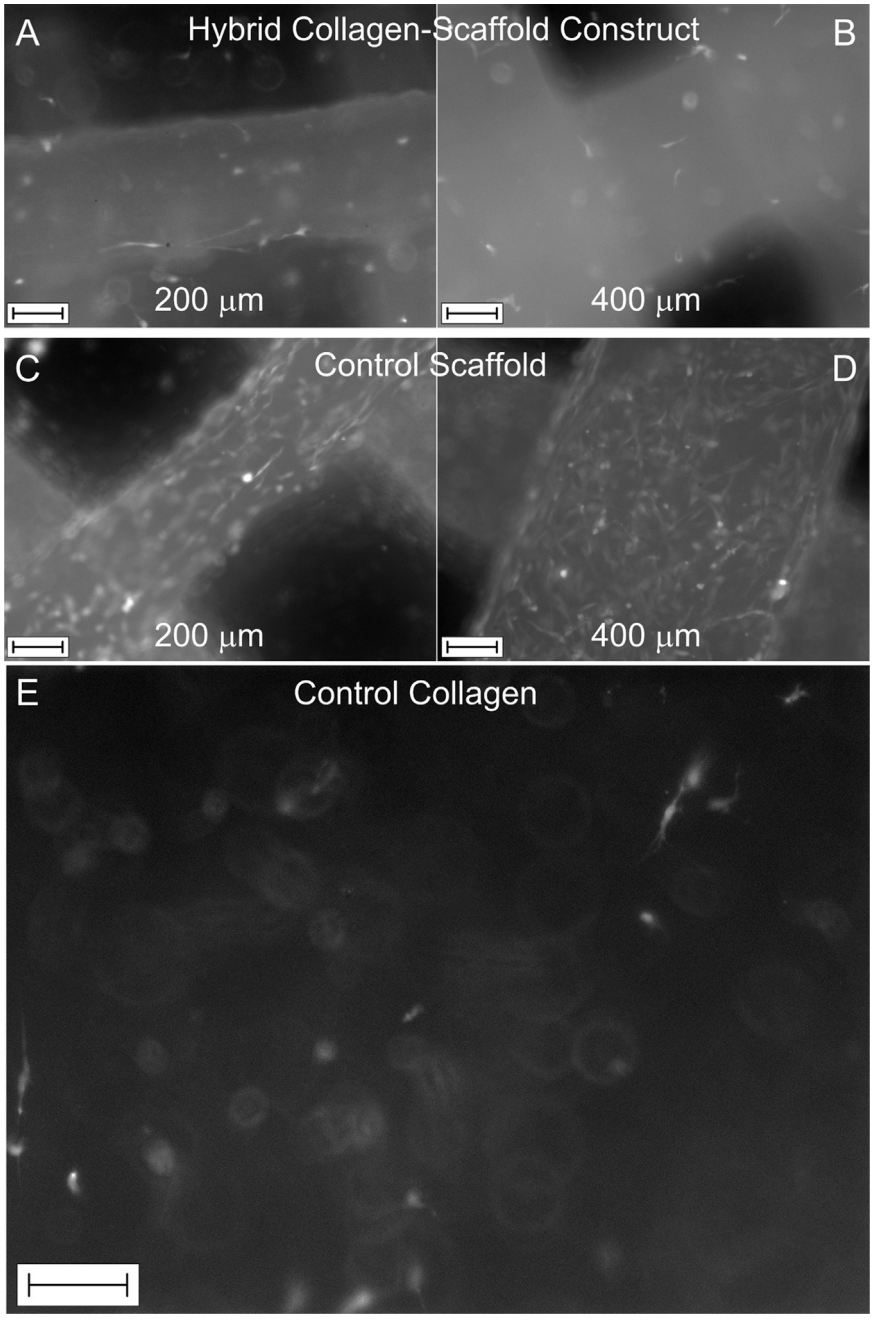

Fig. 3 – Micrograph of (A) and (B) hybrid collagen/PCL-β-TCP constructs, (C) and (D) control PCL-β-TCP scaffolds and (E) control collagen matrix: (A) and (B) GFP-tagged HUVECs evenly distributed in the collagen component of the hybrid constructs after 6 h of collagen loading. (C) and (D) Cells seeded on the control PCL-β-TCP scaffolds. On 200 -μm struts, cells spread, oriented and stretched align with the strut direction. In contrast, cells obtained random orientation tightly enveloping the entire circumference of the struts on the 400 -μm scaffolds. (E) Incorporated HUVECs were evenly distributed and started to spread within control collagen matrix.

30–60% re-growths were observed by day 14. There was no significant difference in cell population between hybrid constructs and control collagen groups. Also, Fig. 2(B) shows that, after 1 day of culture, only about 2% of the initial cells migrated and attached to the scaffold of the hybrid construct. After 14 days of incubation, the total numbers of cells on the struts increased about 265% for 200-μm constructs and 453% for 400-μm constructs as a result of both cell migration towards to the struts and cell proliferation on the struts. Although the total number of cells on the control PCL-β-TCP scaffolds was significantly less than the hybrid constructs (including both collagen and scaffold component), it was much higher than the scaffold's component in the hybrid

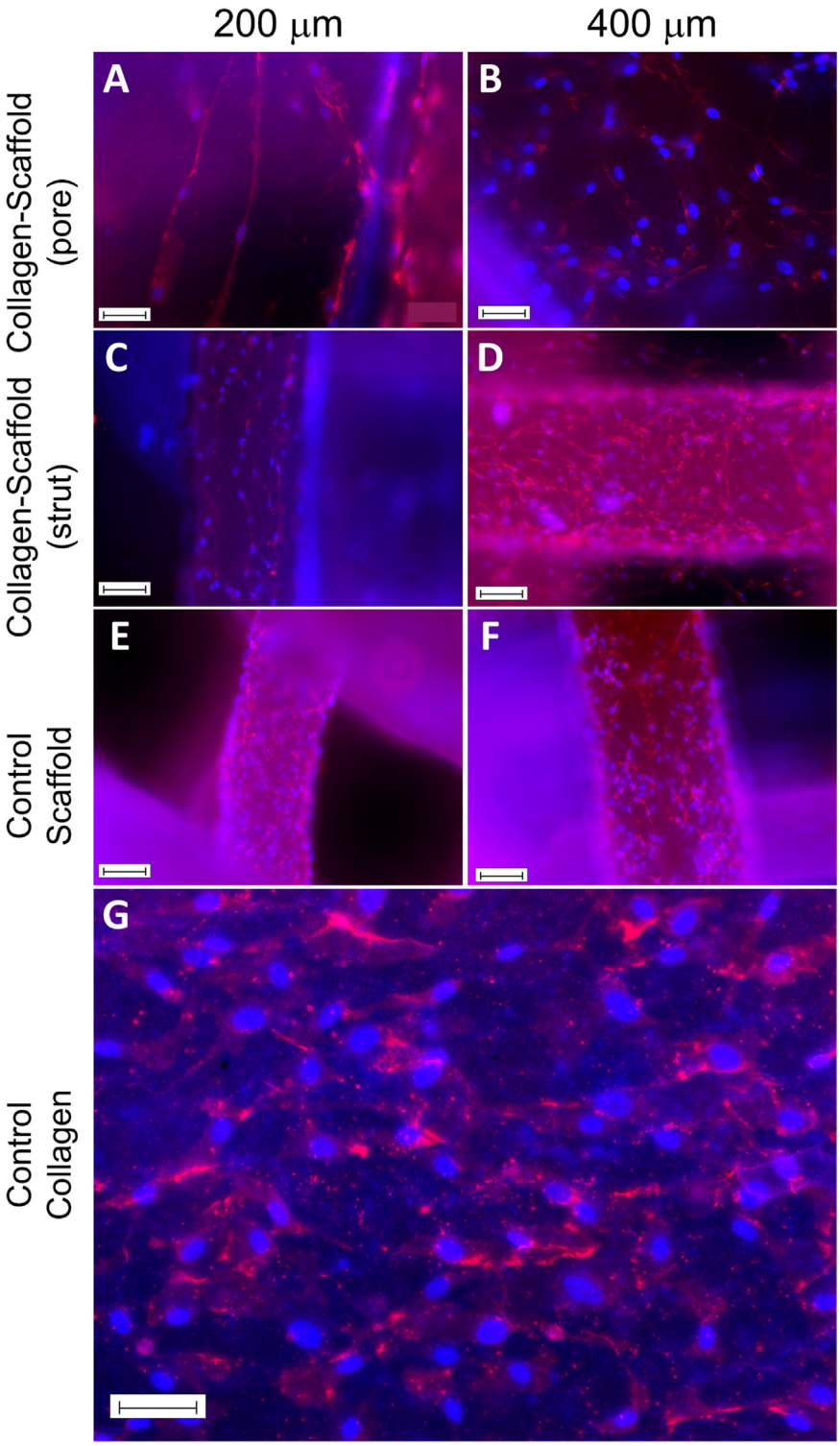

Fig. 4 – HUVECs expressing PECAM-1 (CD 31 – depicted in red, nuclear counterstaining in blue) via immunocytochemical staining after 14 days culture: (A) and (B) cells formed extensive network and cords in the collagen component within the pores of both 200- and 400 -μm hybrid constructs. Cells are elongated and aligned as linear cords in the 200-μm constructs whereas they are randomly-oriented capillary-like in the 400 -μm constructs. Bars equal to 50 μm. (C) On the 200 -μm struts of the hybrid constructs, HUVECs formed network with well-established branches. Bar equals to 100 μm. (D) Many cells adhered on 400 -μm struts of hybrid constructs but no network is detectable. Bar equals to 100 μm. (E) and (F) On control PCL-β-TCP scaffolds, endothelial cells formed a monolayer but no obvious network is observed. Bars equals to 100 μm. (G) HUVECs developed extensive, but random networks in the control collagen matrix. Bar equals to 50 μm. (For interpretation of the references to color in this figure legend, the reader is referred to the web version of this article.)

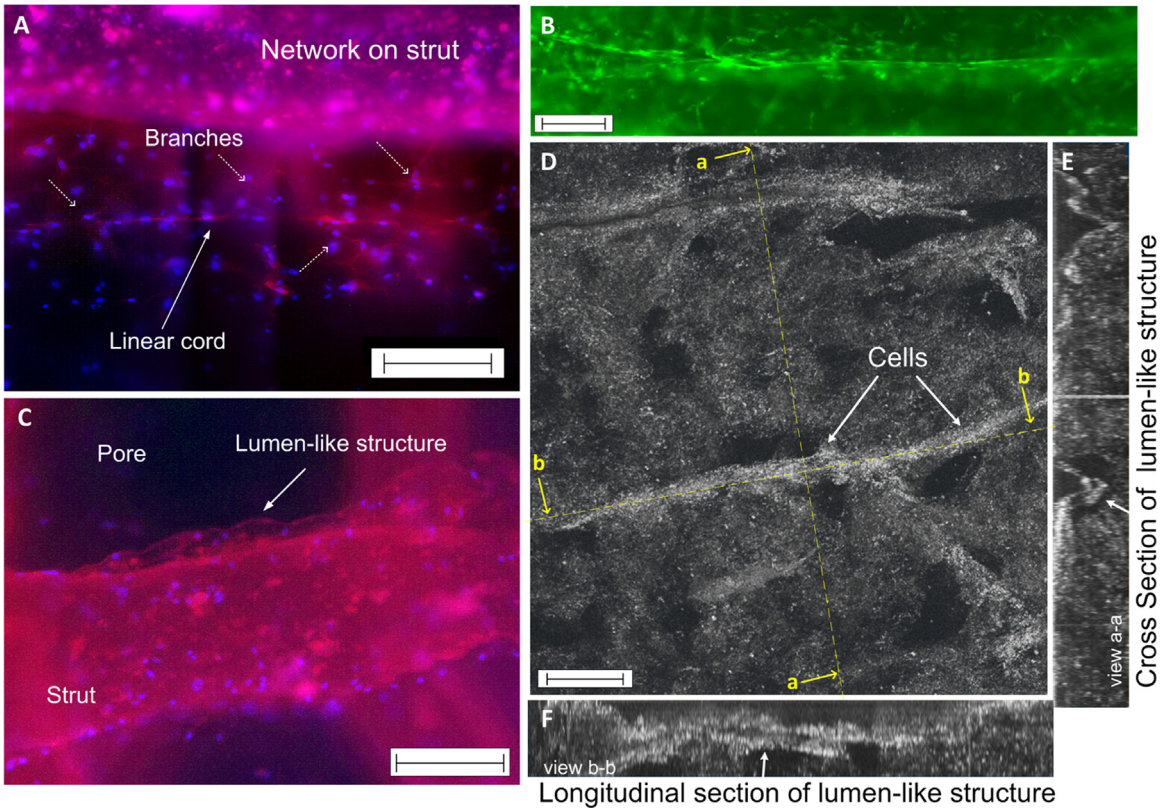

Fig. 5 – Endothelial pattern in the hybrid collagen/PCL-β-TCP construct observed by different methods: (A – fluorescent micrographs of cells with F-actin filaments stained at day 7) HUVECs aligned to form linear cords with branches connected to the primitive capillary-like network in collagen and on the PCL-β-TCP struts, (B - fluorescent micrographs of GFP-tagged cells at day 14) long linear HUVECs cords formed around the scaffolds component and aligned with the struts, (C – fluorescent micrographs of cells expressing CD31 at day 14) well-developed lumen-like structures formed at the interface of the collagen and strut of the 200 -μm scaffold, (D – high resolution OCT at day 14) topography of the top surface of the hybrid construct. (E) cross and (F) longitudinal sections (a-a and b-b) of a lumen-like structures formed within 50 μm depth. White pixels represent cells and dark pixels surrounded by the white pixels represents middle hollow region. Bars equal to 200 μm for A, B, and C. Bar equals to 50 μm for D, E and F.

construct (i.e., about 5-fold at day 14). Cell densities on 200- and 400-μm scaffold components of hybrid TECs were ~1/20 and 1/5 of those of control scaffolds at day 1 and 14, respectively.

3.4. *Morphology, organization and CD31 expression of cells*

The endothelial cell-laden collagen solution was easily infiltrated into and remained within the pores of the surface-treated scaffolds. After gelation, the collagen could be held by the scaffold in air and did not detach, suggesting the bulk mechanical interlock between the scaffold and collagen components. Fig. 3A and B show the morphology of the GFP-tagged cells in the collagen/PCL-β-TCP constructs with 200- and 400 -μm struts, respectively, after 6 h of seeding. HUVECs were observed evenly distributed in the collagen component of the hybrid constructs. Fig. 3C–E, respectively, show the morphology of the GFP-tagged cells on 200- and 400-μm struts of PCL-β-TCP control scaffolds and in the control collagen hydrogel, after 6 h of seeding. Also, as shown in Fig. 3(C), in comparison with 400-μm struts, relatively higher cell density attached, spread, and oriented aligned with the strut direction on the 200-μm struts. Cells also attached well on 400-μm struts, but they appeared with random orientation (Fig. 3(D)). Cell morphology in the control collagen was similar to those in the collagen component of the hybrid constructs.

Fig. 4 shows immunofluorescence images of cell-cell interface and network formation of endothelial cells after 14 days of incubation. PECAM-1 (CD 31) is a cell adhesion molecule present predominantly at the intercellular adherence junctions and stained in red, and nuclei were counterstained in blue. HUVECs formed extensive network in the collagen component within the pores of both 200- and 400-μm hybrid constructs (Fig. 4(A) and (B)), but cells are aligned as linear cords in the 200 -μm constructs whereas they are randomly-oriented and capillary-like in the 400-μm constructs. Also, HUVECs attached onto the 200 -μm struts of the hybrid constructs, and self-assembled to networks that were aligned with the strut orientation (Fig. 4(C)). However, HUVECs did not yield an obvious alignment orientation or form networks on the 400-μm strut (Fig. 4(D)). In addition, in control PCL-β-TCP scaffolds, although endothelial cells proliferated well on the struts after 14 days of culture, no obvious network

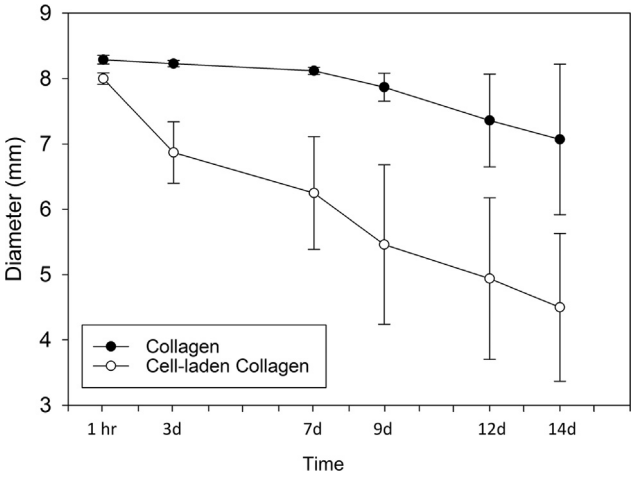

Fig. 6 – Variation of the diameter of cell-laden and cell-free collagen discs over time up to 14 days in culture condition ($n=3$). Cell laden-collagen started to shrink from early hours and to approximately 14% in diameter by day 3, 22% by day 7, and 44% after 14 days of incubation. However, the control collagen disks without cells did not show any significant change up to 7 days and then shrank approximately 15% by day 14 that was probably due to material degradation.

formed (Fig. 4(E) and (F)). HUVECs developed extensive, but random networks in the collagen matrix (Fig. 4(G)).

Fig. 5 collectively demonstrates tubular cords and lumen-like structures formed in collagen/PCL-β-TCP hybrid constructs observed by different methods. Fig. 5(A) shows fluorescent micrographs of HUVECs with F-actin filaments stained at day 7 that were aligned to form linear cords with branches connected to the primitive capillary-like network in collagen and the cells on the PCL-β-TCP struts. Also, long linear tubular cords formed by GFP-tagged HUVECs are shown in Fig. 5(B) depicted from the region around the scaffolds component. In addition, Fig. 5(C) shows that cells expressing CD31 developed lumen-like structures at the interface of the collagen and the 200-μm strut at day 14. Also, Fig. 5 (D) demonstrates a high resolution OCT view of a 50-μm deep top region of a 200-μm hybrid construct with two cross sections (a-a and b-b views) showing a lumen-like structure formed within the collagen component.

3.5. *Dimension changes of collagens in presence and absence of cells*

The variation in the diameter of cell-laden collagen disks in the presence and absence of cells over time was measured as an indicator of the bulk effect of cellular traction force on the collagen matrix. As shown in Fig. 6, the cell-laden collagen started to shrink from early hours and to approximately 14% in diameter by day 3, 22% by day 7, and 44% after 14 days of incubation. However, the control collagen disks without cells did not show any significant change up to 7 days and then shrank approximately 15% by day 14, probably due to material degradation. The difference between cell-laden collagen and control collagen (i.e., ~20% and ~30% dimension change at days 7 and 14, respectively) is probably a result of cellular traction force before day 7 and the combination of cellular traction force and matrix degradation by day 14.

3.6. *Finite element modeling of mechanical stresses*

The traction force acted by the cells on the collagen component of hybrid construct was simulated via a finite element method. The model was validated by predicting the alignment of HUVECs in the collagen hydrogel (Knapp et al., 1999). Fig. 7(A) is a schematic drawing of hybrid constructs, and Fig. 7(B) shows two perpendicular cross-section OCT images of a hybrid construct illustrating how the collagen component is mechanically restricted by the scaffold component in the hybrid construct. Only the two top layers of scaffold component within the cell-laden collagen component are depicted in Fig. 7(B).

The contours of principal mechanical stresses within the collagen component were obtained across the construct as shown from the top view in Fig. 7(C) for 200- and 400-μm hybrid constructs and control collagen-only sample. As seen, linear patterns of principal stresses appeared in the regions surrounding both 200- and 400-μm scaffolds. However, unlike the 200-μm samples, such linear patterns did not form within the pores of 400-μm scaffolds. The simulated pattern of principal stresses highly matched with the pattern of the cell network and the linear cellular cords observed via fluorescent microscopy as depicted in Fig. 7(C) on the selected regions shown by dashed boxes. Also, the values of the principle stress in N/m^2 are shown on selected points/contours. The stresses in the similar regions are higher in 200-μm constructs compared to 400-μm constructs. The stresses in control collagen are much less than the hybrid constructs. No dominant orientation was observed in the network of HUVECs in the control collagen matrix.

4. Discussion

To engineer prevascularized bone TEC, material composition and internal architecture are essential biological and mechanical cues, and need to be properly selected and appropriately tailored, respectively, to guide the organization of cells. In our previous studies, we have demonstrated the importance of rigid porous scaffold to protect structural integrity and functionality of cell-laden hydrogel-based microvasculature (Kang et al., 2015; Chen et al., 2012). In the present study, we combined the PCL-β-TCP scaffold with HUVEC-laden collagen and studied their interaction in an attempt to promote endothelial cell organization and network formation in a hybrid construct. We used AM technology to fabricate mechanically-sound scaffolds of well-defined structure, i.e., controlled pore size, strut size, and lattice pattern. We found that the combination of soft cell-laden collagen hydrogel with rigid PCL-β-TCP scaffold significantly enhanced cell retention compared to scaffolds alone (Fig. 4) and improved hydrogel-based structural and mechanical integrity compared to collagen alone (Fig. 1(E) and (F)). Furthermore, hybrid constructs with relatively thinner struts (relative to pore size) exhibited development of long cords in the pores along scaffold struts compared to those with larger struts; that, in turn, promoted the formation of cellular networks (Figs. 4, 5 and 7). The result

implies that manipulation of scaffold architecture such as strut size, pore size and pattern may be an effective means of regulation and re-organization of endothelial cells for further prevascularization.

A few studies have reported the HUVEC behaviors in hybrid constructs. (Gong et al., 2007; Melchels et al., 2012; Schuurman et al., 2011; Kim et al., 2012; Mintz and Cooper 2014; de Moraes et al., 2012; Santos et al., 2008; Temple et al.,

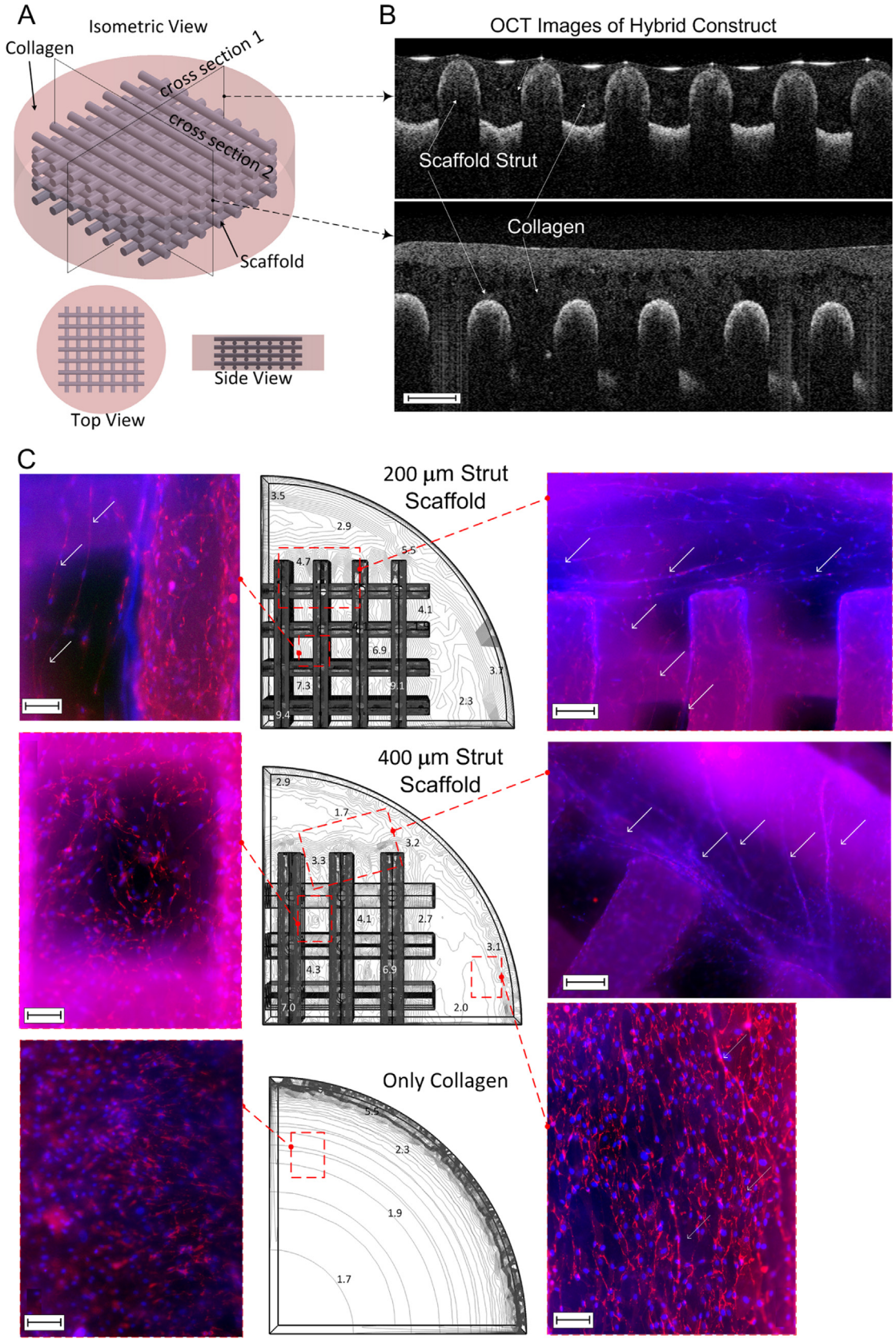

2014). For example, Santos et al. (2008) developed ECM-inspired nano/micro-fiber scaffolds made via an electrospinning technique and pre-seeded endothelial cells onto porous scaffolds and then impregnated them with angiogenic growth factor-incorporated collagen gel. They observed that the cells were able to migrate from the scaffold into the gel matrix and form capillary-like structures. Most recently, Temple et al. loaded fibrin encapsulating 50–300-μm human adipose-derived stem cell aggregates into the AM-made porous PCL scaffolds (Temple et al., 2014). They reported extensive vascular network of random orientation throughout the fibrin-filled scaffold pores, but cellular patterns near PCL struts often appeared wrapped along the struts. Our results in this study are consistent with these previous studies but further indicated that the well-defined internal architecture of a rigid porous scaffold can be a means to regulate the endothelial cell network formation. By taking advantages of AM technology, we were able to control architectural features of porous scaffolds including strut and pore sizes (Table 1) that, in turn, determined their physical properties such as porosity and surface area (Table 2) and influenced their mechanical properties (Fig. 1(E)). The compressive mechanical strength of the fabricated PCL-β-TCP scaffolds were measured in the range resembling the strength of trabecular bone (An, 2000). Since the mechanical stiffness of collagen is orders of magnitude less than scaffold (Fig. 1(E) and (F)), collagen/PCL-β-TCP hybrid constructs demonstrate mechanical stiffness similar to the scaffold component.

In the collagen/PCL-β-TCP hybrid constructs, collagen initially acted as a cell carrier where endothelial cells were directly suspended in collagen hydrogel solution at a relatively high cell density prior to loading onto the scaffolds and gelation. Collagen itself is an extracellular matrix which provides a conducive, physiologically-relevant microenvironment for cells to grow and interact. At day 1, the majority of cells remained highly viable within both collagen components of hybrid constructs and control collagens. However, the total amount of cells declined at day 7, and then re-grew at day 14 (Fig. 2). The decline at day 7 is probably a result of cellular necrosis in the center of constructs of 8 mm in diameter and 3-mm thick due to limited nutrient supplies (Miller et al., 2012). The re-growth at day 14 is probably a result of cell proliferation in the periphery of the constructs where the cells can secure sufficient nutrients and oxygen. It is a known phenomenon for cells encapsulated in hydrogel matrices due to low nutrient and waste transport in regions of the hydrogels far from the culture media (Miller et al., 2012; Chan et al., 2010). To overcome this issue, through channels can be introduced in the hydrogel component in future studies.

After gelation, collagen formed mechanical interlocks with alkaline-treated scaffold struts and stabilized the interface, though PCL-β-TCP scaffold struts are remarkably stiffer and harder compared to collagen hydrogel. This fact may have encouraged cells to migrate onto the scaffold struts since a rigid substrate provides a more stable anchorage and higher stress on cells, while the soft hydrogel will readily facilitate cells to migrate within the 3D collagen matrix. As a result, many cells have migrated from the collagen gel onto the scaffold struts, spread and started to proliferate (Fig. 2 and Supplementary Figs. 1 and 2). HUVECs initiated to form connections on the 200-μm struts by day 7 and established more cell networks by day 14. However, on the 400-μm struts, although cells proliferated and formed a highly confluent layer, no network was observed after 14 days of incubation (Fig. 4). This observation might be explained by the influence of the architectural features of the scaffolds. With a constant pore size of ~500 μm, scaffolds with 200-μm struts (that are comparatively smaller than spacing between the struts) demonstrated higher porosity, water up-take and specific surface area compared to 400-μm scaffolds (Table 2). This means that within the hybrid constructs, the collagen matrix had more interface area with PCL-β-TCP struts of 200-μm scaffolds in comparison with 400-μm scaffolds. Also, the number of cells counted on the struts were similar for 200- and 400-μm struts (Fig. 2), the cellular density (number of cells/surface area) was lower on the 200-μm struts that might have contributed to formation of a better network. Another possible explanation may be a preferred orientation and elongation of cells along the main axis of the 200-μm struts that was stimulated by the smaller radius of curvature compared to that of 400-μm struts, which relatively resemble a flat surface for HUVECs. However, it should be noted that, despite formation of a high density monolayer of HUVECs on the struts of control scaffolds (Fig. 2) and even initial elongation of cells along the 200 -μm struts (Fig. 3(C)), no network was detected on the control scaffolds at day 14 (Fig. 4(E)). A proper biological and mechanical microenvironment at the interface of PCL-β-TCP struts with collagen hydrogel might be a possible reason for the better network formation in the hybrid constructs.

The majority of HUVECs, which remained in the collagen matrix, continued to grow and form more connections by 14 days of culture. However, unlike the control collagen matrix that demonstrated random cellular network, cells made long linear cords within the pores of 200-μm struts as well as within ~800 μm distance surrounding the scaffold component of the hybrid constructs (Figs. 4, 5 and 7). Those long linear cords formed branches and connected to the cell network on the scaffold strut (Fig. 5(A)). Although long cords

Fig. 7 – Analysis of mechanical stresses generated by cellular traction force in collagen component of hybrid constructs. The patterns of principal stresses are compared with the pattern of HUVECs network: (A) schematic of the hybrid constructs, (B) two perpendicular OCT cross sections of a hybrid construct showing two top layers of scaffold component within the cell-laden collagen component. (C) contours of second principal stress patterns for 200 -μm, 400 -μm TECs and control collagen matrix simulated via FEM. The values of the principle stress (in N/m^2) are shown on selected points. Fluorescent micrographs of stained HUVECs at the regions which are determined by dashed boxes are shown, resembling the simulated stress patterns. Long linear cords are depicted by the arrows.

were also seen surrounding 400-μm scaffolds in the hybrid constructs, such linear organization of cells was not detected within the pores of those scaffolds. HUVECs formed random-pattern network within the pores of 400-μm hybrid constructs similar to what was observed in control collagen (Fig. 4).

An active mechano-sensing/mechano-transduction mechanism (Zhang et al., 2011; Janmey and McCulloch, 2007), a positive mechanical feedback loop via transmission of force between the cells and collagen micro-structure (Stopak and Harris, 1982; Ma et al., 2013), may possibly explain the organization of the cellular network in the hybrid scaffold-collagen constructs and the formation of a linear cord structure. In many applications that involve entrapping cells in gels, the cells compact the gel and produce aligned fiber patterns (Stopak and Harris, 1982; Aghvami et al., 2013; Sawhney and Howard, 2002; Provenzano et al., 2008; Bischofs et al., 2008). It is the nanometer-size fibrillar structure of collagen that provides physical cues for cell proliferation and migration to organize and form a new 3D capillary network (Knapp et al., 1999; Davis and Senger, 2005). The fibrillar structure of collagen hydrogel is determined by the polymerization conditions including collagen concentration and pH (Roeder et al., 2002). A recent study by Guo et al. (2012), showed how the morphological changes of epithelial cells in the presence of collagen influences the formation of long cell cords pattern. The motile cells use their traction force to align the collagen fibers and to organize themselves spatially (Namy et al., 2004). The collagen fibers reorganized to form long linear patterns and restricted the cells along those linear patterns (Guo et al., 2012). In turn, elongated ECs will have increased sensitivity to growth factors in the culture media (Folkman and Shing, 1992). Also, the encapsulated cells, passed the effective traction forces onto surrounding collagen hydrogel matrix in the bulk scale (Grinnell and Petroll, 2010) and formed mechanical stress within the collagen matrix based on the mechanical stiffness of the matrix and the boundary mechanical constrains (Sieminski et al., 2004; Ingber, 2002; Klumpers et al., 2013). In the hybrid constructs, the collagen matrix is mechanically constrained at the interface with the culture well and at the integration interface with the scaffold struts. The cell-generated mechanical stresses within the collagen matrix are transmitted back and act on the cells (Knapp et al., 1999; Ingber, 2002; Grinnell, 2000; van Oers et al., 2014) that regulate cellular functions and capillary morphogenesis (Sieminski et al., 2004).

We indirectly estimated the strength of cellular traction force acted by the encapsulated HUVECs on the collagen matrix via measuring their effect on the bulk size of collagen disks (Fig. 6). The results suggested a remarkably strong internal force introduced by the cell traction force (~20% shrinkage difference between cell-laden collagen and control collagen without cells at day 7). We also used FEM to simulate the formation of stresses caused by the traction force of the incorporated cells within the collagen matrix of the soft hydrogel/rigid scaffold hybrid constructs. Interestingly, the pattern of principal stress directions highly matched with the pattern of the HUVEC network observed in the collagen component of the hybrid constructs for both 200- and 400-μm struts (Fig. 7). Thus, the main rationale behind the linear pattern of HUVECs network in the pores of 200-μm struts versus the random pattern of cells in the pores of 400-μm struts may be attributed to the pattern of generated mechanical stress by cellular traction. The relative aspect ratio of the actual fabricated strut size (~260 and 442 μm – Table 1) in comparison with the actual pore size (~440 μm – Table 1) might be the main rationale behind this difference between the generated mechanical stress patterns. It has been shown by others (Tambe et al., 2011) that cells align with the orientation of the principal stresses and also migrate along that orientation. Other than elongation of cells and network pattern, mechanical constrains might have also affected the lumen size, as Sieminski et al. (2004) showed that HUVECs formed larger lumens in mechanically constrained collagen gel. Cell population might have also played a critical role for the initiation of the mechano-transduction mechanism as mentioned in literature (Chan et al., 2010; Guo et al., 2012; Barocas et al., 1998). A higher number of cells means more traction force and consequently higher stresses and more aligned fibers. For this study, we used a high initial density of 5×10^6 cells/ml that showed the potential to generate relatively high contraction in the collagen matrix (Fig. 6). In a hybrid construct, the rigid scaffold component maintained the overall geometry, meaning it acted as a mechanical constrain resulting in formation of high mechanical stress in the collagen component and consequently on the incorporated cells.

The results suggest that the integration of the AM-made rigid PCL-β-TCP scaffold with thin struts and cell-laden soft collagen hydrogel not only benefited from hydrogel-based cell retention and structural integrity, but also promoted the formation of long linear cords branched and connected to the smaller networks (Fig. 5) via reciprocal mechano-transduction effects (Fig. 7). Formation of such cellular patterns that resemble the vascular network pattern may facilitate the formation of capillary network with porous TECs. Whether the developed linear cords and cellular pattern could enable development of vascular network and further anastomosis and blood flow within the constructs upon implantation will be investigated in future work using both *in vitro* and *in vivo* animal models. In addition, the cellular necrosis in the core region of large TEC could be solved using flow of culture medium in the channel embedded constructs *in vitro* and anastomosis to host vasculature system *in vivo* that will be our studies in future work (Mercado-Pagan et al., 2015). Also, this study can be extended through analysis of effective parameters such as the scaffold architectural design, chemical composition/concentration of the scaffold and hydrogel components, and different cell type. Co-culturing osteogenic cells with angiogenic cells in the hybrid construct could be investigated in future work.

5. Conclusion

In this study, we combined endothelial cell-laden soft hydrogel with AM-made rigid porous scaffold and studied endothelial network pattern initiation in the hybrid construct. It was

shown that the hybrid constructs with thinner scaffold struts promoted cell reorganization and initial network formation composed of long linear cords connected to capillary-like branches. Scaffold struts modulated the patterns of principal stresses within the collagen and influenced the cell organization and network formation.

Acknowledgment

This work was supported by grants from the following agencies: NIH R01AR057837 (NIAMS), NIH R01DE021468 (NIDCR), DOD W911NF-14-1-0545 (DURIP), DOD W81XWH-10-1-0966 (PRORP), DOD W81XWH-10-200-10, and Wallace H. Coulter Foundation. The authors would like to express their appreciation to A. Behn (Department of Orthopedic Surgery, Stanford University) for technical assistance and Mrs. Tahereh Marvdashti (Department of Electrical Engineering, Stanford University) for assistance with low-resolution OCT imaging.

Appendix A. Supplementary material

Supplementary data associated with this article can be found in the online version at http://dx.doi.org/10.1016/j.jmbbm.2016.08.037.

REFERENCES

Aghvami, M., Barocas, V.H., Sander, E.A., 2013. Multiscale mechanical simulations of cell compacted collagen gels. J Biomech. Eng. 135 (7), 71004.

An, Y.H., 2000. Mechanical properties of bone. In: An, Y.H., Draughn, R.A. (Eds.), Mechanical Testing of Bone and the Bone-Implant Interface. CRC Press, Boca Raton, Florida, pp. 50–51.

Auger, F.A., Gibot, L., Lacroix, D., 2013. The pivotal role of vascularization in tissue engineering. Annu. Rev. Biomed. Eng. 15 (1), 177–200.

Barocas, V.H., Girton, T.S., Tranquillo, R.T., 1998. Engineered alignment in media equivalents: magnetic prealignment and mandrel compaction. J. Biomech. Eng. 120 (5), 660–666.

Bischofs, I.B., Klein, F., Lehnert, D., Bastmeyer, M., Schwarz, U.S., 2008. Filamentous network mechanics and active contractility determine cell and tissue shape. Biophys. J. 95 (7), 3488–3496.

Cen, L., Liu, W., Cui, L., Zhang, W., Cao, Y., 2008. Collagen tissue engineering: development of novel biomaterials and applications. Pediatr. Res. 63 (5), 492–496.

Chan, V., Zorlutuna, P., Jeong, J.H., Kong, H., Bashir, R., 2010. Three-dimensional photopatterning of hydrogels using stereolithography for long-term cell encapsulation. Lab Chip 10 (16), 2062–2070.

Chen, X., Aledia, A.S., Ghajar, C.M., Griffith, C.K., Putnam, A.J., Hughes, C.C., SC. G, 2009. Prevascularization of a fibrin-based tissue construct accelerates the formation of functional anastomosis with host vasculature. Tissue Eng. Part A 15 (6), 1363–1371.

Chen, Y.C., Lin, R.Z., Qi, H., Yang, Y., Bae, H., Melero-Martin, J.M., Khademhosseini, A., 2012. Functional human vascular network generated in photocrosslinkable gelatin methacrylate hydrogels. Adv. Funct. Mater. 22 (10), 2027–2039.

Correia, C., Grayson, W.L., Park, M., Hutton, D., Zhou, B., Guo, X.E., Niklason, L., Sousa, R.A., Reis, R.L., Vunjak-Novakovic, G., 2011. In vitro model of vascularized bone: synergizing vascular development and osteogenesis. PLoS One 6 (12), e28352.

Davis, G.E., Senger, D.R., 2005. Endothelial extracellular matrix: biosynthesis, remodeling, and functions during vascular morphogenesis and neovessel stabilization. Circ. Res 97 (11), 1093–1107.

Deng, C., Zhang, P., Vulesevic, B., Kuraitis, D., Li, F., Yang, A.F., Griffith, M., Ruel, M., Suuronen, E.J., 2010. A collagen-chitosan hydrogel for endothelial differentiation and angiogenesis. Tissue Eng. Part A 16 (10), 3099–3109.

Duffy, G.P., McFadden, T.M., Byrne, E.M., Gill, S.L., Farrell, E., O'Brien, F.J., 2011. Towards in vitro vascularisation of collagen – GAG scaffolds. Eur. Cell Mater. 21, 15–30.

Fedorovich, N.E., Haverslag, R.T., Dhert, W.J., Alblas, J., 2010. The role of endothelial progenitor cells in prevascularized bone tissue engineering: development of heterogeneous constructs. Tissue Eng. Part A 16 (7), 2355–2367.

Folkman, J., Shing, Y., 1992. Angiogenesis, J. Biol. Chem. 267 (16), 10931–10934.

Garvin, K.A., Dalecki, D., Hocking, D.C., 2011. Vascularization of three-dimensional collagen hydrogels using ultrasound standing wave fields. Ultrasound Med Biol. 37 (11), 1853–1864.

Gong, Y., He, L., Li, J., Zhou, Q., Ma, Z., Gao, C., Shen, J., 2007. Hydrogel-filled polylactide porous scaffolds for cartilage tissue engineering. J. Biomed. Mater. Res B: Appl. Biomater. 82 (1), 192–204.

Grinnell, F., 2000. Fibroblast-collagen-matrix contraction: growth-factor signalling and mechanical loading. Trends Cell Biol. 10 (9), 362–365.

Grinnell, F., Petroll, W.M., 2010. Cell motility and mechanics in three-dimensional collagen matrices. Annu. Rev. Cell Dev. Biol. 26, 335–361.

Guo, C.L., Ouyang, M., Yu, J.Y., Maslov, J., Price, A., Shen, C.Y., 2012. Long-range mechanical force enables self-assembly of epithelial tubular patterns. Proc. Natl. Acad. Sci. USA 109 (15), 5576–5582.

Hanjaya-Putra, D., Bose, V., Shen, Y.I., Yee, J., Khetan, S., Fox-Talbot, K., Steenbergen, C., Burdick, J.A., Gerecht, S., 2011. Controlled activation of morphogenesis to generate a functional human microvasculature in a synthetic matrix. Blood 118 (3), 804–815.

Ingber, D.E., 2002. Mechanical signaling and the cellular response to extracellular matrix in angiogenesis and cardiovascular physiology. Circ. Res. 91 (10), 877–887.

Janmey, P.A., McCulloch, C.A., 2007. Cell mechanics: integrating cell responses to mechanical stimuli. Annu. Rev. Biomed. Eng. 9 (1), 1–34.

Kang, Y., Mochizuki, N., Khademhosseini, A., Fukuda, J., Yang, Y., 2015. Engineering a vascularized collagen-β-tricalcium phosphate graft using an electrochemical approach. Acta Biomater. 11, 449–458.

Kang, Y.Q., Mochizuki, N., Khademhosseini, A., Fukuda, J., Yang, Y.Z., 2015. Engineering a vascularized collagen-beta-tricalcium phosphate graft using an electrochemical approach. Acta Biomater. 11, 449–458.

Kim, M., Hong, B., Lee, J., Kim, S.E., Kang, S.S., Kim, Y.H., Tae, G., 2012. Composite system of PLCL scaffold and heparin-based hydrogel for regeneration of partial-thickness cartilage defects. Biomacromolecules 13 (8), 2287–2298.

Klumpers, D.D., Zhao, X., Mooney, D.J., Smit, T.H., 2013. Cell mediated contraction in 3D cell-matrix constructs leads to spatially regulated osteogenic differentiation. Integr. Biol. 5 (9), 1174–1183.

Knapp, D.M., Tower, T.T., Tranquillo, R.T., Barocas, V.H., 1999. Estimation of cell traction and migration in an isometric cell traction assay. AIChE J. 45 (12), 2628–2640.

Leong, M.F., Toh, J.K., Du, C., Narayanan, K., Lu, H.F., Lim, T.C., Wan, A.C.A., Ying, J.Y., 2013. Patterned prevascularised tissue constructs by assembly of polyelectrolyte hydroel fibers. Nat. Commun. 4, 2353.

Levenberg, S., Rouwkema, J., Macdonald, M., Garfein, E.S., Kohane, D.S., Darland, D.C., Marini, R., van Blitterswijk, C.A., Mulligan, R.C., D'Amore, P.A., et al., 2005. Engineering vascularized skeletal muscle tissue. Nat. Biotechnol. 23 (7), 879–884.

Lim, H.C., Bae, J.H., Song, H.R., Teoh, S.H., Kim, H.K., Kum, D.H., 2011. High tibial osteotomy using polycaprolactone-tricalcium phosphate polymer wedge in a micro pig model. J. Bone Jt. Surg. – Br. 93 (1), 120–125.

Lloyd-Griffith, C., McFadden, T.M., Duffy, G.P., Unger, R.E., Kirkpatrick, C.J., O'Brien, F.J., 2015. The pre-vascularisations of a collagen-chondroitin sulphate scaffold using human amniotic fluid-derived stem cells to enhance and stabilise endothelial cell-mediated vessel formation. Acta Biomater. 26, 263–273.

Lovett, M., Lee, K., Edwards, A., DL. K, 2009. Vascularization strategies for tissue engineering. Tissue Eng. Part B Rev. 15 (3), 353–370.

Ma, X.Y., Schickel, M.E., Stevenson, M.D., Sarang-Sieminski, A.L., Gooch, K.J., Ghadiali, S.N., Hart, R.T., 2013. Fibers in the extracellular matrix enable long-range stress transmission between cells. Biophys. J. 104 (7), 1410–1418.

Macedo, F., Nunes, E., Vasconcelos, W., Santos, R., Sinisterra, R., Cortes, M., 2012. A biodegradable porous composite scaffold of PCL/BCP containing Ang-(1-7) for bone tissue engineering. Cerâmica 58 (348), 481–488.

McFadden, T.M., Duffy, G.P., Allen, A.B., Stevens, H.Y., Schwarzmaier, S.M., Plesnila, N., Murphy, J.M., Barry, F.P., Guldberg, R.E., O'Brien, F.J., 2013. The delayed addition of human mesenchymal stem cells to pre-formed endothelial cell networks results in functional vascularization of a collagen-glycosaminoglycan scaffold in vivo. Acta Biomater. 9 (12), 9303–9316.

Melchels, F.P.W., Domingos, M.A.N., Klein, T.J., Malda, J., Bartolo, P.J., Hutmacher, D.W., 2012. Additive manufacturing of tissues and organs. Prog. Polym. Sci. 37 (8), 1079–1104.

Mercado-Pagan, A.E., Stahl, A.M., Shanjani, Y., Yang, Y., 2015. Vascularization in bone tissue engineering constructs. Ann. Biomed. Eng. 43 (3), 718–729.

Miller, J.S., Stevens, K.R., Yang, M.T., Baker, B.M., Nguyen, D.H., Cohen, D.M., Toro, E., Chen, A.A., Galie, P.A., Yu, X., et al., 2012. Rapid casting of patterned vascular networks for perfusable engineered three-dimensional tissues. Nat. Mater. 11 (9), 768–774.

Mintz, B.R., Cooper Jr., J.A., 2014. Hybrid hyaluronic acid hydrogel/poly(varepsilon-caprolactone) scaffold provides mechanically favorable platform for cartilage tissue engineering studies. J. Biomed. Mater. Res. A 102 (9), 2918–2926.

de Moraes, M.A., Paternotte, E., Mantovani, D., Beppu, M.M., 2012. Mechanical and biological performances of new scaffolds made of collagen hydrogels and fibroin microfibers for vascular tissue engineering. Macromol. Biosci. 12 (9), 1253–1264.

Mota, C., Puppi, D., Chiellini, F., Chiellini, E., 2015. Additive manufacturing techniques for the production of tissue engineering constructs. J. Tissue Eng. Regen. Med. 9 (3), 174–190.

Namy, P., Ohayon, J., Tracqui, P., 2004. Critical conditions for pattern formation and in vitro tubulogenesis driven by cellular traction fields. J. Theor. Biol. 227 (1), 103–120.

Provenzano, P.P., Inman, D.R., Eliceiri, K.W., Trier, S.M., Keely, P.J., 2008. Contact guidance mediated three-dimensional cell migration is regulated by Rho/ROCK-dependent matrix reorganization. Biophys. J. 95 (11), 5374–5384.

Roeder, B.A., Kokini, K., Sturgis, J.E., Robinson, J.P., Voytik-Harbin, S.L., 2002. Tensile mechanical properties of three-dimensional type I collagen extracellular matrices with varied microstructure. J. Biomech. Eng. 124 (2), 214–222.

Sakaguchi, K., Shimizu, T., Horaguchi, S., Sekine, H., Yamato, M., Umezu, M., Okano, T., 2013. In vitro engineering of vascularized tissue surrogates. Sci. Rep. 3, 1316.

Santos, M.I., Tuzlakoglu, K., Fuchs, S., Gomes, M.E., Peters, K., Unger, R.E., Piskin, E., Reis, R.L., Kirkpatrick, C.J., 2008. Endothelial cell colonization and angiogenic potential of combined nano- and micro-fibrous scaffolds for bone tissue engineering. Biomaterials 29 (32), 4306–4313.

Sawhney, R.K., Howard, J., 2002. Slow local movements of collagen fibers by fibroblasts drive the rapid global self-organization of collagen gels. J. Cell Biol. 157 (6), 1083–1091.

Sawyer, A.A., Song, S.J., Susanto, E., Chuan, P., Lam, C.X.F., Woodruff, M.A., Hutmacher, D.W., Cool, S.M., 2009. The stimulation of healing within a rat calvarial defect by mPCL–TCP/collagen scaffolds loaded with rhBMP-2. Biomaterials 30 (13), 2479–2488.

Schuurman, W., Khristov, V., Pot, M.W., van Weeren, P.R., Dhert, W.J., Malda, J., 2011. Bioprinting of hybrid tissue constructs with tailorable mechanical properties. Biofabrication 3 (2), 021001.

Shanjani, Y., Pan, C.C., Elomaa, L., Yang, Y., 2015. A novel bioprinting method and system for forming hybrid tissue engineering constructs. Biofabrication 7 (4), 045008.

Sieminski, A.L., Hebbel, R.P., Gooch, K.J., 2004. The relative magnitudes of endothelial force generation and matrix stiffness modulate capillary morphogenesis in vitro. Exp. Cell Res. 297 (2), 574–584.

Stopak, D., Harris, A.K., 1982. Connective tissue morphogenesis by fibroblast traction. I. Tissue culture observations. Dev. Biol. 90 (2), 383–398.

Tambe, D.T., Hardin, C.C., Angelini, T.E., Rajendran, K., Park, C.Y., Serra-Picamal, X., Zhou, E.H., Zaman, M.H., Butler, J.P., Weitz, D.A., et al., 2011. Collective cell guidance by cooperative intercellular forces. Nat. Mater. 10 (6), 469–475.

Temple, J.P., Hutton, D.L., Hung, B.P., Huri, P.Y., Cook, C.A., Kondragunta, R., Jia, X., Grayson, W.L., 2014. Engineering anatomically shaped vascularized bone grafts with hASCs and 3D-printed PCL scaffolds. J Biomed. Mater. Res. A 102 (12), 4317–4325.

Tian, L., George, S.C., 2011. Biomaterials to prevascularize engineered tissues. J. Cardiovasc. Transl. Res. 4 (5), 685–698.

van Oers, R.F., Rens, E.G., LaValley, D.J., Reinhart-King, C.A., Merks, R.M., 2014. Mechanical cell-matrix feedback explains pairwise and collective endothelial cell behavior in vitro. PLoS Comput. Biol. 10 (8), e1003774.

Wu, C.C., Ding, S.J., Wang, Y.H., Tang, M.J., Chang, H.C., 2005. Mechanical properties of collagen gels derived from rats of different ages. J. Biomater. Sci. Polym. Ed. 16 (10), 1261–1275.

Yang, S., Leong, K.F., Du, Z., CK. C, 2002. The design of scaffolds for use in tissue engineering. Part II. Rapid prototyping techniques. Tissue Eng. 8 (1), 1–11.

Yeo, A., Wong, W.J., Khoo, H.H., Teoh, S.H., 2010. Surface modification of PCL-TCP scaffolds improve interfacial mechanical interlock and enhance early bone formation: an in vitro and in vivo characterization. J. Biomed. Mater. Res. A 92 (1), 311–321.

Yeo, A., Rai, B., Sju, E., Cheong, J.J., Teoh, S.H., 2008. The degradation profile of novel, bioresorbable PCL-TCP scaffolds: an in vitro and in vivo study. J. Biomed. Mater. Res. A 84 (1), 208–218.

Yeo, M., Simon, C.G., Kim, G., 2012. Effects of offset values of solid freeform fabricated PCL–β-TCP scaffolds on mechanical properties and cellular activities in bone tissue regeneration. J. Mater. Chem. B 22 (40), 21636.

Zarnescu, L., Leung, M.C., Abeyta, M., Sudkamp, H., Baer, T., Behr, B., Ellerbee, A.K., 2015. Label-free characterization of vitrification-induced morphology changes in single-cell embryos with full-field optical coherence tomography. J. Biomed. Opt. 20 (9), 096004.

Zein, I., Hutmacher, D.W., Tan, K.C., Teoh, S.H., 2002. Fused deposition modeling of novel scaffold architectures for tissue engineering applications. Biomaterials 23 (4), 1169–1185.

Zhang, H., Landmann, F., Zahreddine, H., Rodriguez, D., Koch, M., Labouesse, M., 2011. A tension-induced mechanotransduction pathway promotes epithelial morphogenesis. Nature 471 (7336), 99–103.